NMR investigation of water diffusion in different biofilm structures

Authors: Maria P. Herrling, Jessica Weisbrodt, Catherine M. Kirkland, Nathan H. Williamson, Susanne Lackner, Sarah L. Codd, Joseph D. Seymour, Gisela Guthausen, & Harald Horn.

Herrling MP, J. Weisbrodt, Catherine M. Kirkland, N.H. Williamson, S. Lackner, Sarah L. Codd,Joseph D. Seymour, G. Guthausen, H. Horn, “NMR Investigation of Water Diffusion in different Biofilm Structures,” Biotechnol Bioeng 114, no.12 (September 4, 2017): 2857-2867. doi:10.1002/bit.26392.

NMR investigation of water diffusion in different biofilm structures

Maria P. Herrling Jessica Weisbrodt Catherine M. Kirkland
Nathan H. Williamson Susanne Lackner Sarah L. Codd
Joseph D. Seymour Gisela Guthausen Harald Horn

INTRODUCTION

Abstract

Mass transfer in biofilms is determined by diffusion. Different mostly invasive approaches have been used to measure diffusion coefficients in biofilms, however, data on heterogeneous biomass under realistic conditions is still missing. To non-invasively elucidate fluid–structure interactions in complex multispecies biofilms pulsed field gradient-nuclear magnetic resonance (PFG-NMR) was applied to measure the water diffusion in five different types of biomass aggregates: one type of sludge flocs, two types of biofilm, and two types of granules. Data analysis is an important issue when measuring heterogeneous systems and is shown to significantly influence the interpretation and understanding of water diffusion. With respect to numerical reproducibility and physico-chemical interpretation, different data processing methods were explored: (bi)-exponential data analysis and the Γ distribution model. Furthermore, the diffusion coefficient distribution in relation to relaxation was studied by D-T_2 maps obtained by 2D inverse Laplace transform (2D ILT). The results show that the effective diffusion coefficients for all biofilm samples ranged from 0.36 to 0.96 relative to that of water. NMR diffusion was linked to biofilm structure (e.g., biomass density, organic and inorganic matter) as observed by magnetic resonance imaging and to traditional biofilm parameters: diffusion was most restricted in granules with compact structures, and fast diffusion was found in heterotrophic biofilms with fluffy structures. The effective diffusion coefficients in the biomass were found to be broadly distributed because of internal biomass heterogeneities, such as gas bubbles, precipitates, and locally changing biofilm densities. Thus, estimations based on biofilm bulk properties in multispecies systems can be overestimated and mean diffusion coefficients might not be sufficiently informative to describe mass transport in biofilms and the near bulk.

KEYWORDS

biofilm, effective diffusion coefficient, gamma distribution, mass transport, PFG-NMR

Biofilms or more generally biomass aggregates are pervasive in natural aquatic systems (Costerton, Lewandowski, Caldwell, Korber, & Lappinscott, 1995; Sutherland, 2001) as well as in technical systems (Metcalf & Eddy, 2003). Their substrate conversion depends on bulk and internal structures influencing the mass transfer into the matrix. Generally, this mass transfer in biomass aggregates is driven by

diffusion and plays a key role for metabolic activity (Flemming & Wingender, 2010; Stewart, 2003; Wäsche, Horn, & Hempel, 2002). The investigation and understanding of mass transfer and substrate consumption is essential for the development of strategies to improve design and operation of biofilm-based technical applications as well as for modeling. In-depth knowledge is required—especially for multi-species biofilms under technical and realistic conditions.

To experimentally explore fluid–structure interactions, several analytical methods have been applied. Imaging techniques (Neu et al., 2010) and micro-sensors (Billings, Birjiniuk, Samad, Doyle, & Ribbeck, 2015; Guimera et al., 2016) have been used the most. Furthermore, mathematical modeling leads to mechanistic understanding of mass transfer phenomena in complex biofilm systems (Horn & Lackner, 2014). Biofilm modeling in combination with imaging indicates that rough biofilms show higher mass transfer of substrates compared to smooth biofilms under stagnation conditions. The larger interfacial surface of a rough biofilm provides better contact to substrates (Li, Wagner, Lackner, & Horn, 2016). The diffusion coefficient D of substrates into the biofilm is assumed constant over the biofilm depth (IWA, 2006). In transport models, D is usually set to 20–30% less than D_{water} (IWA, 2006). Diffusion of water and nutrients strongly varies between different biofilm systems, geometries, and growth conditions. Actual mass fluxes inside biofilms are unknown, and a generalization of mass transport is not possible. Therefore, data on heterogeneous systems are needed to address measures for mass transport in real systems. Pulsed-field gradient nuclear magnetic resonance (PFG-NMR) allows the measurement of translational diffusion completely non-invasively and non-destructively (Callaghan, 1991, 2011), also in micro-porous systems and in restricted geometry.

In biofilm research, alginate is often used as model system due to the chemical composition which is comparable to the biofilms' extracellular polymeric substances (EPS). Gel heterogeneities were detected in transverse relaxation T_2 maps (Fabich et al., 2012). Filtration processes have been imaged in hollow fiber membranes using alginate as model system (Arndt, Roth, Nirschl, Schütz, & Guthausen, 2016). Basic knowledge gained from investigations of artificial biofilms can be transferred to real biofilm systems. Monoculture and multispecies biofilms were investigated by NMR flow and diffusion in porous media and flow cells to study water dynamics and biofilm growth at different time and length scales (Herrling, Guthausen, Wagner, Lackner, & Horn, 2015; Manz, Volke, Goll, & Horn, 2005; Seymour, Gage, Codd, & Gerlach, 2004, 2007; Vogt, Sanderlin, Seymour, & Codd, 2013). Furthermore, combined diffusion and Magnetic Resonance Imaging (MRI) linked mass transfer to biofilm structure (Manz et al., 2005; Neu et al., 2010). Diffusion strongly depends on biofilm systems, growth conditions, and biofilm geometries. For example, in methanogenic granular sludge internal heterogeneities significantly influenced the mass transfer (Lens et al., 2003). Strong correlations between the diffusion of substrates and biofilm parameters have been reported (Bishop, Zhang, & Fu, 1995; Debeer, Stoodley, Roe, & Lewandowski, 1994; Stewart, 2003). For example, Renslow et al. (2010) correlated the effective diffusion coefficient with biofilm depth by means of PFG-NMR and imaging in *Shewanella oneidensis* biofilms. The same was found for phototrophic *Phormidium* biofilms (Ramanan, Holmes, Sloan, & Phoenix, 2013). Other studies also confirm that D is biofilm-specific and depth-dependent with a linear decrease of D with biofilm depth (McLean, Ona, & Majors, 2008; Phoenix & Holmes, 2008).

Mass transport and diffusion in biofilms are difficult to analyze and to model because of the high complexity of these biomass aggregates. Apart from the influence of specific compounds, PFG-NMR measurements and data interpretation deserve scrutiny. Different data processing approaches are summarized in Röding et al. (2012) and Röding, Williamson, and Nydén (2015). The most commonly used data processing approach for PFG-NMR data is the (bi)-exponential fit. Diffusion coefficients are obtained by fitting a single exponential function to the measured signal attenuation, leading to effective or apparent diffusion coefficients. An alternative and recently introduced approach is the **Γ** distribution model which offers mean diffusion coefficients and their distribution width. Different data processing schemes are compared for biomass aggregates in this study to show their limitations and relevance. For mathematical description, we refer to Röding et al. (2012, 2015). Water diffusion coefficients in multispecies biofilms with diverse geometries and data processing schemes are compared in this paper. To identify fluid–structure interactions, five different types of biofilms or biomass aggregates were investigated: sludge flocs, fluffy and compact biofilms grown on carriers, and aerobic and (an)aerobic granules. The goals of the study were to (i) characterize the biomass by means of physico-chemical parameters and imaging; (ii) compare D_{water} in different structures to identify correlations between biomass properties and water diffusion; and (iii) compare PFG-NMR data processing schemes, including (bi)-exponential fit, **Γ** distribution, and 2D inverse Laplace transform.

2 | MATERIALS AND METHODS

2.1 | Sample preparation of biomass aggregates

Activated sludge flocs, carrier based biofilms, and granules were chosen to cover a broad range of physical morphologies which are technically relevant, for example, for wastewater treatment. The properties and functionalities are summarized in Table 1. Sludge flocs (sludge) were collected from a full-scale wastewater treatment plant in Weinheim (Germany). The sludge is a mixed culture of auto- and heterotrophic biomass used for carbon (C), nitrogen (N), and phosphorus (P) removal from wastewater. The sludge was rinsed and sieved to a size fraction <200 μm prior to characterization. Two different carrier based biofilms were investigated. Fluffy biofilms (biofilm_1) grown on K1 carrier materials (plastic carrier, diameter: 10 mm, AnoxKaldnes, Sweden) were cultivated in a laboratory-scale moving bed biofilm reactor fed with acetate (Herrling et al., 2016). Biofilm_1 comprised heterotrophic biomass and was mainly used for removal of easily degradable carbon compounds. Compact biofilms (biofilm_2) on K3 (plastic carrier, diameter: 25 mm, AnoxKaldnes, Sweden) were obtained from a full-scale wastewater treatment plant (AnoxKaldnes' Biofarm) in Malmö, Sweden. Biofilm_2 comprised

TABLE 1 Characterization of the biofilms

Parameter	Sludge	Biofilm_1	Biofilm_2	Granules_1	Granules_2
Micro-organisms	Auto-/heterotrophic	Heterotrophic	Autotrophic	Auto-/heterotrophic	Mainly autotrophic
Removal	C/N/P	C	N	C/N/P	N/C
TSS in the reactor	6 g/L TSS	86 mg TSS/carrier	270 mg TSS/carrier	40 mg TSS/granule	3 g/L TSS
VSS [%]	80	90	69	78	80
Biofilm thickness [μm]	<200*	<200	<1,000	10,000*	700–900*
Biofilm density [g/L]	1,033 ± 15	–	1,047 ± 4	1,029 ± 2	1,046 ± 14
Ca [g/kg TSS]	37	–	490	97	286
P [g/kg TSS]	53	–	132	49	72
Fe [g/kg TSS]	37	–	590	0.6	327
S [g/kg TSS]	10	–	6	6.8	84
Si [g/kg TSS]	2	–	65	0.2	37

Data marked with asterisk (*) refer to diameter of the granules. "C" refers to carbon removal, "N" to nitrogen removal, and "P" to phosphorous removal. The density of water at 20°C is 998 g/L.

multiple species, that is, heterotrophs, nitrifiers, denitrifiers, and anammox bacteria (Gilbert et al., 2014) and was mainly used for N removal. Two different types of granules, that is, granulated biofilms, were also selected for the investigation. Aerobic granules (granules_1) were cultivated in a laboratory-scale sequencing batch reactor (SBR) with acetate as the main substrate. Granules_1 were used for N, P, and easily degradable C removal. Large sized granules with an approximate diameter of 10 mm were manually selected. Additionally, (an)aerobic granules (granule_2) were collected from a side-stream SBR of a full-scale wastewater treatment plant in Heidelberg (Germany). Granules_2 mainly contributed to the removal of N and some slowly degradable C compounds. Granules_2 were rinsed and sieved to a size fraction of 700–900 μm. All biofilms were rinsed prior to the experiment to remove particulate matter and stored in tap water at 4°C. Biofilms were imaged by light microscope SMT4 (Mikroskop Technik Rathenow) in combination with a DSLR camera (Canon EOS 600D) and characterized by their total suspended solid concentration (TSS) and volatile suspended solid concentration (VSS) according to DIN-EN-12880 (2001). The biomass density was determined by pycnometer measurement ($n = 4$, 10 ml, Blaubrand) according to DIN ISO 35079 and the solids density was calculated according to Loosdrecht, Nielsen, Lopez-Vazquez, and Brdjanovic (2016). Element analysis was conducted by atomic emission spectroscopy (ICP-OES, Varian VistaPro, Agilent Technologies, l detection limit: 10 μg/L) after acid digestion. ICP-OES data for biofilm_1 are not available due to low biofilm mass.

2.2 | MRI and PFG-NMR

2.2.1 | MRI

MRI experiments were performed on a 200 MHz MRI instrument (Bruker Avance 200 SWB, Bruker BioSpin GmbH, Rheinstetten, Germany) with a magnetic flux B_0 of 4.7 T, 150 mm vertical bore and equipped with a Bruker gradient system micro 2.5 and a ^{1}H-NMR bird-cage (25 mm inner diameter). All measurements were performed temperature controlled at 25°C using the Bruker software ParaVision. The often used multi-slice multi-echo imaging sequence (MSME) (Callaghan, 1991; Kimmich, 1997) was applied to acquire predominantly proton density-weighted images due to the minimum echo time used in the experiments. The biofilms were imaged using the same acquisition parameters as in a previous study (Ranzinger et al., 2016) with $T_R = 10$ s, $\tau_E = 50$ ms, number of averages = 4, pixel matrix 128 × 128, slice thickness 0.8 mm. To maintain the original structure, sludge and granules_2 were filled into glass vials with 1 ml of tap water from Karlsruhe to avoid osmotic stress. The Karlsruhe tap water (average values of 2015, Stadtwerke Karlsruhe) had a pH of 7.2, total organic carbon concentration of 0.84 mg/L and an electrical conductivity of 653 μS/cm (c (Ca^{2+}) = 110 mg/L, c (Na^+) = 11.1 mg/L, c (K^+) = 1.7 mg/L, c (Cl^-) = 22.8 mg/L, c (HCO^-) = 232 mg/L).

Wet biofilm_1, biofilm_2, and granules_1 were placed into plastic wrap (without bulk water) and directly inserted into the bird-cage. The measured signal intensity is encoded on a gray-scale and physically corresponds to the proton density, slightly weighted by the transverse relaxation T_2. The slightly T_2-weighted proton density images allow the discrimination of the main components within the biofilm system, being either ^{1}H containing liquid (signal) or solid or gas (no signal intensity in MSME images). Additionally, materials without ^{1}H, that is, minerals, do not show up in the ^{1}H images.

2.3 | Diffusion measurements

Translational motion was measured by PFG-NMR, that is, the pulsed application of magnetic field gradients which encode and decode the position across an ensemble of molecules at different times. The time between the encoding and decoding pulses is the diffusion time Δ. The PFG-NMR acquisition parameters are summarized in Table 2. Biomass samples were measured using the PFG stimulated echo (PFG-STE) (Callaghan, 2011) on the above described NMR spectrometer equipped with the Bruker software Topspin and a Diff30 probe,

TABLE 2 Acquisition parameters for PFG-NMR diffusion measurements

Acquisition parameter	Measurement I PFG-STE	Measurement II PFG-STE	Measurement III D_T_2_STE
Gradient pulse duration	3 ms	1 ms	1.136 ms
Diffusion time	40, 100, 200, 400, 500, 800 ms	50, 100, 200 ms	100 ms
First rf pulse delay	4.26 ms	21.21 ms	21.21 ms
Recycle delay	8 s	900 ms	12 s
Diffusion gradient amplitude	0.016–0.5 T/m linear in 32 steps	−0.32 to +0.32 T/m linear in 64 steps	0.015–0.2 T/m linear in 64 steps
Number of scans	4	16	32
Number of dummy scans	1	0	4
Gradient direction	*z*	*z*	*z*

Measurement I was applied to all biofilm samples. Measurements II and III were used to characterize biofilm_1.

which allowed *z*-gradients *g* of up to 12 T/m. Acquisition parameters were chosen according to Table 2, measurement I. The logarithmic, normalized signal attenuation $\ln(S/S_0)$ was measured as a function of q, where $q = \gamma\delta g$, γ being the gyromagnetic ratio, δ the gradient pulse duration, and g the gradient amplitude. Complementary measurements were performed on a 250 MHz MRI tomograph (Bruker Avance 250 SWB, Bruker BioSpin GmbH, Rheinstetten, Germany) also equipped with a Diff30 Probe (maximum gradient 17 T/m) employing acquisition parameters of measurements II and III, (Table 2). Images taken at the beginning and end of the experiments showed stable biofilm structure. All diffusion measurements were performed as single measurements at 25°C.

2.4 | Data processing

2.4.1 | (Bi)-exponential model

D_{water} was obtained by fitting a single exponential function to the measured signal attenuation as it is expected for a homogeneous liquid of small molecules (Callaghan, 1991). In the biofilm matrix, the motion of water is partially restricted. The samples are highly heterogeneous; therefore, a *D*-distribution is expected. However, as little is known about the details and mechanisms, the question about an appropriate model is essential for a confident data interpretation. As a first approach, the commonly used (bi)-exponential function $\frac{S}{S_0} = A_1 \exp\left(-D_1 q^2\left(\Delta - \frac{\delta}{3}\right)\right) + A_2 \exp\left(-D_2 q^2\left(\Delta - \frac{\delta}{3}\right)\right)$ (Eq. 1) with the gradient duration δ. D_1 and D_2 in biofilms were obtained, meaning that there is a fast (D_1) and a slow (D_2) diffusion fraction described by the relative amplitudes A_i. D_1 makes up more than 80% of the signal amplitude and is the dominant part. A small portion with signal amplitudes of 4–20% can be associated with D_2 (in the range of 10^{-10} to 10^{-11} m^2/s), which is significantly lower than D_1. Due to the dominant relative signal amplitude, the discussion focuses on D_1 in the following. The relative effective diffusion coefficient is defined by $f_{D\_exp} = D_1 / D_{water}$ (Eq. 2), which is used to compare the diffusion properties of the samples.

Data were processed using self-written scripts in Matlab® (version R2012a, Matlab Works, Inc.; Natick, MA) which take special care of the small amplitude of the second diffusion contribution. This (bi)-exponential rather than a mono-exponential approach is essential for accurately describing the majority of the data to avoid miss- or over-interpretation due to numerical errors during data processing. Only data points with signal above the noise level were used in the fits.

2.4.2 | Gamma distribution model

For heterogeneous systems, the Stejskal–Tanner approach for self-diffusion of homogeneous liquids composed of small molecules does not apply necessarily. *D*-distributions are physically more meaningful than a discrete number of *D* in these highly complex and heterogeneous systems. Apart from the conventionally used (bi)-exponential function for modeling the signal attenuation, a recently developed approach by Röding et al. (2012, 2015) was used to reveal the distribution of diffusion coefficients. The **Γ** distribution function is a generalization of distribution functions known in mathematical statistics. One of the advantages is that the equation for the experimentally observed magnetization as a function of q^2 becomes rather simple and accurate, for details, we refer to Röding et al. (2012). Data were processed using self-written scripts (Matlab®) to obtain D_{mean} and the distribution width σ. The relative effective diffusion coefficient within the **Γ** distribution is defined by $f_{D\_g} = D_{mean}/D_{mean,\ water}$ (Eq. 3). The ratio between D_{mean}/D_1 listed in Table 4 indicates the difference between the data analysis approaches and underlines the importance of using a physical and numerically appropriate model.

2.4.3 | 2D inverse Laplace transform

Another approach to model data deviating from a strictly mono-exponential behavior is a purely numerical approach, the inverse Laplace transform (ILT). Diffusion measurements can additionally be combined with relaxation measurements, and the data can be Laplace transformed in two dimensions. In the present case, $D - T_2$ maps were obtained by performing a 2D inverse Laplace transform (2D ILT) (Callaghan, Godefroy, & Ryland, 2003; Lee, Labadie, Springer, & Harbison, 1993; Vogt et al., 2013) to correlate diffusion and relaxation measurements for biofilm_1.

3 | RESULTS AND DISCUSSION

3.1 | Biofilm and biomass characterization: Comparison of common quantities and images

Biomass is commonly characterized by, that is, thickness, density, elemental composition, TSS, and VSS, which do not consider spatial and structural inhomogeneities. On the other hand, mass transport and diffusion properties strongly depend on these spatial inhomogeneities but are not unique in the sense of a one-to-one correspondence of structure and diffusion coefficient. In a first approach, the microscopic findings and the macroscopic chemical parameters were collected and compared to link these physical parameters to water diffusion.

As evident in stereomicroscopic and MRI images (Table 3), sludge consisted of a complex, but loose network of flocs with a small-scale heterogeneity. The measured biomass density of 1,033 g/L is within the expected biomass densities for active sludge flocs with 1,020–1,060 g/L (Dammel & Schroeder, 1991) and is higher than pure water density (998 g/L at 20°C). The mineral content was relatively low with 37 g Ca per kg TSS. It is expected that the water diffusion is hindered in the sludge flocs, and is therefore, slower than free water.

Compared to the heterogeneous structure of the sludge flocs, biofilm_1 comprised a fluffy and homogenous structure (Table 3). The fluffiness of the biofilm is indicative for the low biofilm density (not distinguishable from free water) and high VSS of 90%. The pycnometer measurements for biofilm_1 were not reproducible due to low density and low biomass concentration. Furthermore, spatial variation in biomass density, which influences water dynamics in the biomass, cannot be captured by a simple pycnometer measurement. Another approach is to get insight into the biomass structure and density by MRI. MRI image contrast delivers qualitative information: biofilm_1 was visible in the slightly T_2-weighted images due to the reduced T_2 in the biofilm compared to bulk water. This effect is based mainly on the exchange of protons between EPS biopolymers (mainly OH-groups) and water molecules (Sanderlin, Vogt, Grunewald, Bergin, & Codd, 2013) as well as by the different molecular mobility of molecules in biofilm matrix and water. In proton-density weighted images, biofilm_1 was hardly distinguishable from bulk water because of similar proton concentration (Ranzinger et al., 2016). Based on this knowledge, the density was estimated to be ~1,010 g/L.

Biofilm_2 was cultivated for ~12 months in a WWTP, TSS, and mineral accumulation were significantly higher than in all other biofilms, therefore, diffusion is expected to be highly restricted. The iron content was especially high due to iron-accumulating bacteria (anammox) (Gilbert et al., 2014). The internal structure was heterogeneous: outer biofilm layers were less dense than layers close to the carrier material reflected in the gray values of corresponding MRI voxels. Solids (precipitates, possibly $CaCO_3$) and gas bubbles (air, CO_2, N_2 gas due to microbial activity) appear black with the usual phase susceptibility artifacts. The local heterogeneities in biofilm structure can be related to advanced biofilm age, density, and growth conditions. Those heterogeneities suggest that there are regions in the biofilm which for which water diffusion is restricted to a larger extent than in other regions.

Under certain cultivation conditions, biofilm formation is also possible without carrier material, commonly known as granules. Due to high shear stress applied during cultivation, the surface of granules_1 and granules_2 were compact and smooth. However, in the large granules_1 strong internal heterogeneities became apparent in the MRI images, such as structural layers of microorganisms and precipitates which might lower diffusion in the biomass. The biomass density was within the conventional range for aerobic granules (1,005–1,070 g/L), which depends among others on the cultivation conditions and volume fraction of solid (de Kreuk et al., 2005; Etterer & Wilderer, 2001; Winkler, Kleerebezem, Strous, Chandran, & van Loosdrecht, 2013). Granules with a high solids content of precipitates can have biomass densities up to 1,200 g/L (Juang, Adav, Lee, & Tay, 2010). Granules_2 originated from a WWTP accumulated significantly more minerals (e.g., Ca, P, Fe, P) than granules_1, which were cultivated in a lab scale reactor. Furthermore, biomass density of granules_2 was in the same range as biofilm_2. As density is known to be one of the most important parameters for diffusion in biomass (Renslow et al., 2010), the correlation between usually measured parameters and diffusion coefficients were explored.

3.2 | Diffusion of water in the presence of biomass

To relate biofilm geometry and composition to water diffusion, PFG-NMR diffusion experiments were carried out on different biomasses. As mentioned, the biofilm's heterogeneity poses some challenges for modeling diffusion in these systems. The logarithmic signal attenuation was measured as a function of q^2, results of biofilm_2 and granules_2 are shown in Figure 1 together to provide examples of the data and the numerical fits. Diffusion data from the biofilms were interpreted with both the (bi)-exponential fit (indicated as [bi.]-exp.-func.) and the gamma distribution model (indicated by **Γ** distr.). The levels for good description of the data are depicted in form of 2% and 4% of the maximum amplitude, respectively, corresponding to the goodness of **Γ** distr. fit to the data. A significant difference in the signal attenuation between the samples is evident (inset in Figure 1), which can be explained by the different biomass properties (see Table 1) influencing the water dynamics significantly. The compact morphology and low VSS lead to a reduced water diffusion in granules_2 compared to biofilm_2. The (bi.)-exp.-func. leading to D_1 and D_2 does not describe the measured data sufficiently well, especially the first data points (inset in Figure 1). The reason is found in the discrete approach which is physically not really appropriate for a multicomponent system. A discrepancy results between D_1 (from the [bi.]-exp fit) compared to D_{mean} (from the **Γ** distr. fit). The **Γ** distr. represents the measured data above the noise level significantly better than the (bi.)-exp.-func., resulting in lower residuals leading to a better data quality and higher accuracy. The results for D_1 and D_{mean} differ by 15% (biofilm_2) and 5% (granules_2) which supports the above argument. The findings are in agreement with previously published results for other heterogeneous samples such as motor oils, where a better description of measured diffusion data was achieved by **Γ** distr. (Foerster, Nirschl, & Guthausen, 2017). The importance of an appropriate data analysis is obvious as the

TABLE 3 Summary of stereomicroscopic images and MRI (slightly T_2-weighted image) of the investigated biofilms

Biomass	Stereomicroscopic image	MRI
Sludge	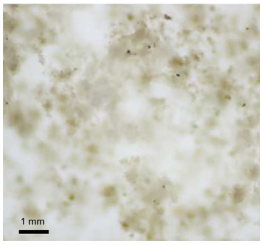	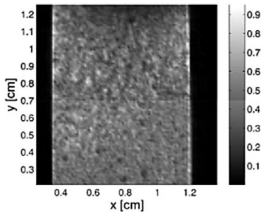
Biofilm_1	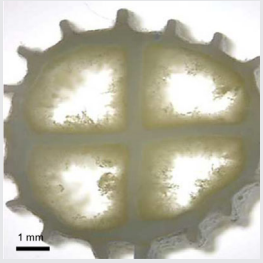	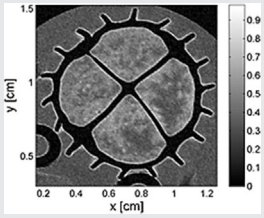
Biofilm_2	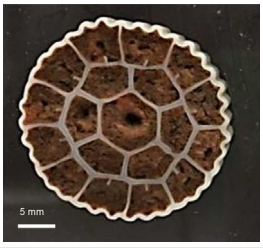	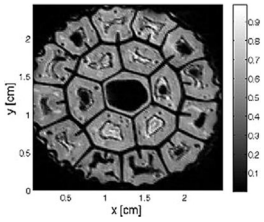
Granules_1		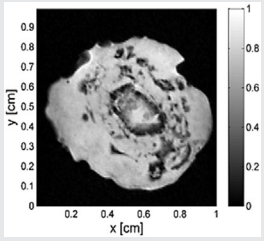
Granules_2	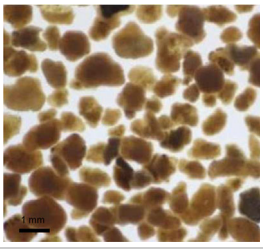	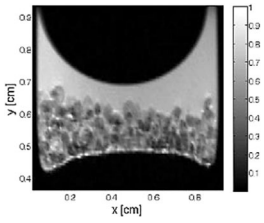

The resolution for MRI images was approximately 100 x 100 μm^2.

diffusion coefficients influence simulation for substrate conversion in biological systems.

3.3 | Influence of biomass structure on water dynamics

D_1 and D_{mean} were obtained by (bi.)-exp.-func. and **Γ** distr., respectively (Table 4). $D_{water} = 2.09\ m^2/s \cdot 10^{-9}$ was slightly lower than the reported values (Renslow et al., 2010; Vogt et al., 2013) due to different water purity and temperature. When comparing the two data processing approaches, D_{mean} and D_1 for water were similar within approximately 2%. D_{mean}/D_1 is close to 1 for free water as expected.

D_1 and D_{mean} measured in the presence of biofilms deviated by 20–30% (D_1/D_{mean} between 0.95 and 1.26). This indicates a good overall agreement for both data processing approaches despite the better fitting of the measured data by **Γ** distribution. D_{mean} is typically slightly larger than D_1 (Table 4) as in the (bi)-exponential fit only D_1 with $A_{rel} > 84\%$ was considered. The minor part of the signal is associated with D_2, which is in the range of 10^{-10} to $10^{-11}\ m^2/s$. D_2 might be assigned to intracellular water (Vogt, Flemming, & Veeman, 2000).

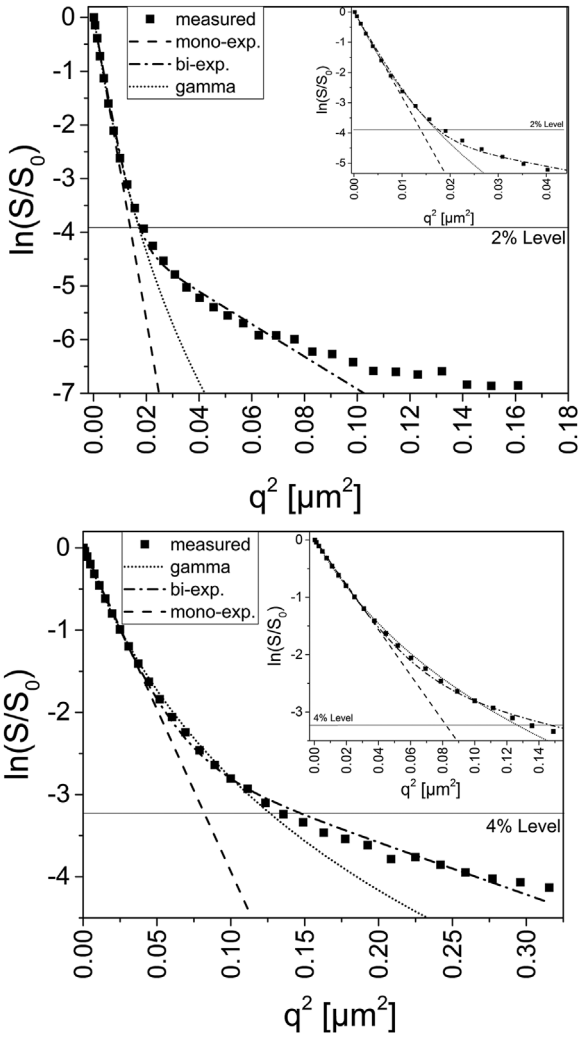

FIGURE 1 The logarithmic signal attenuations of biofilm_2 (top) and granules_2 (bottom) are depicted exemplarily as a function of q^2. The mono- and bi-exponential decay functions and the gamma distribution model were fitted to the data. The levels for good description of the data are depicted in form of 2% and 4% of the maximum amplitude, respectively, corresponding to the goodness of fit of the gamma model to the data. Deviations of the mono-exponential model are evident

Previous studies have also demonstrated that water diffusion coefficients in biofilms are lower than in pure water due to restricted diffusion in the biomass matrix, cells, and EPS, resulting in a wide range of diffusion coefficients between 10^{-9} and 10^{-13} m^2/s (Vogt et al., 2000). f_{D_exp} and f_{D_g} vary strongly with the type of biofilm. The lowest f_{D_g} was found for granules_2 (0.36) and highest f_{D_g} for the biofilm_1 (0.96). Diffusion was most restricted in granules_2 likely due to the compact structure and high content of inorganic matter (Table 1). In comparison, the diffusion coefficients in heterotrophic biofilm_1 were closest to D_{water} because of the fluffy structure and high VSS of 90%. Results are within the typical range of reported relative diffusion coefficients for biofilm from 0.2 to 0.8 (Horn, Reiff, & Morgenroth, 2003; Stewart, 1998; Wood, Quintard, & Whitaker, 2002) except biofilm_1.

In Figure 2, D_1 and D_{mean} are directly compared for the different biofilm samples. The "error" bars for D_{mean} represent the width of the **Γ** distr. σ, listed in Table 4: σ for pure water was very small and not visible, whereas σ for all biofilms was large. Sludge and biofilm_2 show the highest σ possibly due to their highly heterogeneous internal structure (Table 4). The diffusion coefficients D_1 and D_{mean} vary for all biomass, with biofilm_1 showing fastest and granules_2 showing lowest diffusion coefficients. The water diffusion in sludge and biofilm_2 are similar, although the biomass structure parameters differ significantly. As visible in Table 3, these biomasses comprise completely different morphologies being either an open network or a compact biofilm. Furthermore, biomass structural parameters (e.g., VSS, biofilm thickness, and density) differ strongly and suggest that the diffusion in biofim_2 is more hindered than in the sludge. However, this is not the case. This leads to the conclusion that the assumptions regarding mass transfer in biofilms based on bulk physical properties are not directly related to the classical parameters or optical appearance. No clear correlations are found between certain integral biofilm properties and diffusion coefficients: the biofilm thickness and geometry seemed to have a minor influence on D in the present case. For example, biofilm_2 and granules_2 had similar densities, but D differed by approximately 50% when using both data processing methods. Liquid channels in biofilm_2 correspond to an enhanced

TABLE 4 Summary of diffusion coefficients (at Δ 200 ms) in biofilms gained by two different data analysis approaches

Model/ sample	(bi).-exp.-func., D_1 $[m^2/s] \cdot 10^{-9}$	(bi).-exp.-func., f_{D_exp} [−]	Relative amplitude of D_1 contribution, A_{rel} [−]	Γ distr., D_{mean} $[m^2/s] \cdot 10^{-9}$	Γ distr., f_{D_g} [−]	Γ distr. width, σ $[m^2/s] \cdot 10^{-10}$	Ratio, D_{mean}/D_1 [−]
Water	2.09*	1	–	2.04	1	$3.19 \cdot 10^{-3}$	0.98
Sludge	1.45	0.69	0.93	1.62	0.79	8.55	1.11
Biofilm_1	1.76	0.84	0.97	1.96	0.96	5.17	1.12
Biofilm_2	1.47	0.70	0.95	1.69	0.83	7.18	1.15
Granules_1	1.27	0.61	0.94	1.60	0.78	4.96	1.26
Granules_2	0.76	0.36	0.84	0.73	0.36	4.71	0.95

Diffusion coefficients D_1 and D_{mean} obtained by (bi)-exponential fit (indicated by [bi.]-exp.-func.) and gamma distribution (indicated by **Γ** distr.), respectively. Data indicated by asterisk (*) were fitted using mono-exponential function. f_D is the relative effective diffusion coefficient for both data processing approaches (see Eqs. 2 and 3).

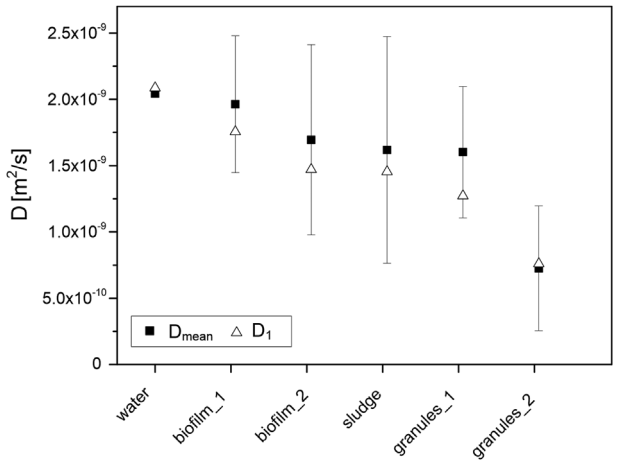

FIGURE 2 Diffusion coefficients D_1 and D_{mean} obtained by (bi)-exponential fit and τ distribution for water and different biomasses measured with a diffusion time Δ = 200 ms. "Error" bars around Dmean represent not statistical errors but the width of the **Γ** distribution σ (see Table 2)

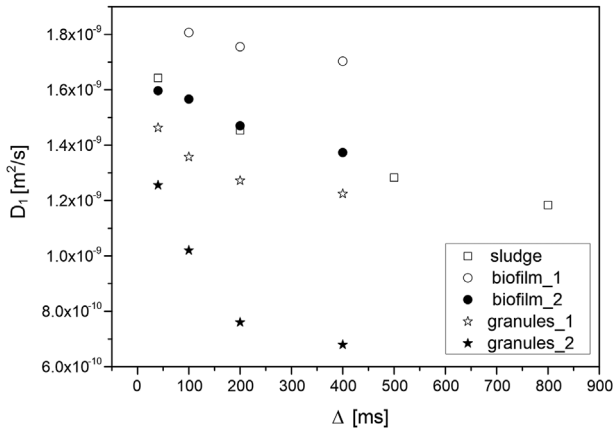

FIGURE 3 Diffusion coefficients D_1 of biofilms at different diffusion times Δ. Classically, the dependence of the diffusion coefficients on diffusion time is a hint on hindered or restricted diffusion and is most pronounced in the granules. Data points for 500 and 800 ms are only given for sludge

water diffusion within the biomass resulting in similar apparent diffusion values as highly porous sludge.

The broad range of relative diffusion coefficients highlights the fact that biofilm structure determines the mass transfer and ultimately the performance of productive biofilms, such as the mentioned wastewater biofilms or fungal bio pellets (Hille, Neu, Hempel, & Horn, 2009). Whether the measured water diffusion can be transferred to relevant substrates for biofilms remains unclear. The substrates' molecular weight, interaction with the surroundings as well as diffusivity and penetration into the biofilm differ from water molecules and could be explored by heteronuclear NMR diffusion measurements and theoretical models can help to answer this question. Using a simple calculation, we estimated the difference between COD (chemical oxygen demand) turnover for the highest (biofilm_1) and lowest (granula_2) diffusion coefficient. The oxygen flux can roughly be estimated by $D/\Delta z^*$ (concentration DO at biofilm surface − concentration DO at z) (Eq. 4), where z is the biofilm depth and DO the dissolved oxygen concentration. D_{mean} was used a diffusion coefficient due to the best fit of the data. Keeping all biofilm related parameters constant (only changing D) the lower diffusion results in 20% less turnover based on flux estimates, thus knowing the diffusion coefficient is highly relevant for biofilm modeling. Further investigations are planned in the future.

Besides that, the results contribute to link transport processes to biofilm structure which was shown for nanoparticle and metal transport in biofilms (Peulen & Wilkinson, 2011; Phoenix & Holmes, 2008). The comparison of classical integral quantities with optical and MRI images shows that the approach of just using one measure for biofilm characterization is insufficient. A comprehensive characterization on different time and length scales is needed when aiming for an understanding of biofilms and the processes of mass transport and especially diffusion. The link between structure, diffusion, and biological activity deserves further research.

3.4 | Influence of diffusion time on water dynamics

In homogeneous liquids of small molecules, D is independent of diffusion time Δ. In porous media, D decreases with increasing Δ due to barriers like physical restriction and adhesion of water molecules (Callaghan, 1991). Biofilms can also be regarded as porous media consisting of biofilm matrix and bulk water. Our results show, that D_1 decreased with Δ for all biofilms (Figure 3). D_1 was selected as the trends were most pronounced. D_{mean} showed a similar but less marked effect. Water diffusion was most restricted in granules_2, indicated by the strong decline of D_1 and low diffusion coefficient asymptote of $6.5\,m^2/s \cdot 10^{-10}$ at 400 ms, followed by granules_1. A different composition of EPS and microbial communities as well as the length scales of the heterogeneous internal structures are already visible in MRI images (Table 3) and are possible explanations for our observations. The mobility of water molecules may also be decreased due to entrapment in EPS molecules (Belton, 1997; Vogt et al., 2000). As already mentioned, sludge and biofilm_2 both displayed fast diffusion, similar distribution width, and a small dependence on Δ. Biofilm_1 did not show a strong diffusion barrier; only a slight decline of D_1 relative to D_{water} was found which leads to the conclusion that

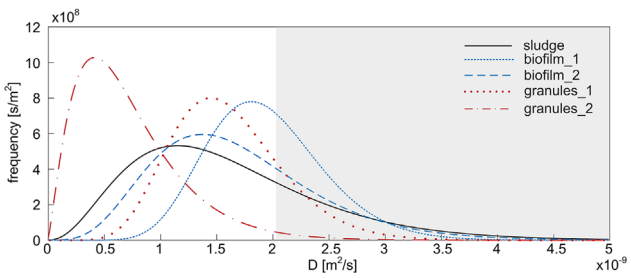

FIGURE 4 Distribution of the diffusion coefficients according to **Γ** distribution. $D = D_{mean}$ for free water is $2.04 \cdot 10^{-09}\,m^2/s$. Gray region indicates diffusion values, which are larger than free water

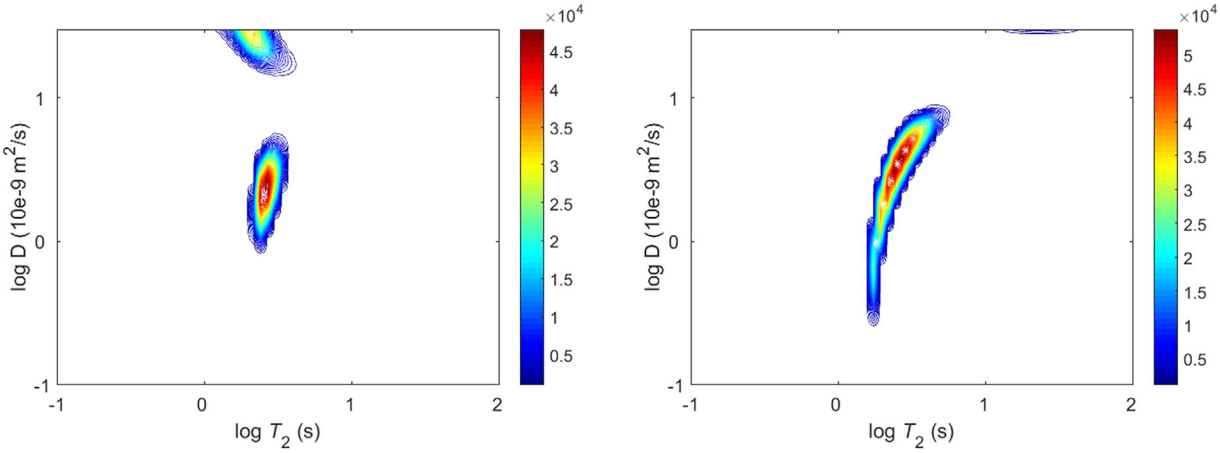

FIGURE 5 Effective diffusion spin-spin relaxation correlation maps for free water (left) and biofilm_1 (right) at a diffusion time of 100 ms. Data were processed using 2D-ILT and reveals the correlation between diffusion and transverse relaxation both being influenced by the structural properties of the biomass

mainly unrestricted bulk water is observed. The calculated D also include the diffusion in the near bulk water which may be influenced by the presence of the biofilm, as has been shown for emulsions (Guan et al., 2010).

The distributions of the effective diffusion coefficients obtained within **Γ** distr. are shown in Figure 4. Granule_2 exhibits the narrowest distribution (σ of 4.71 $m^2/s \cdot 10^{-10}$) together with the slowest D_{mean}. Faster diffusion was found for sludge and biofilm_2 with a broader distribution (σ of 8.55 and 7.18 $m^2/s \cdot 10^{-10}$). Narrow distributions, but with faster D_{mean} were found for biofilm_1 and granules_1. The sludge and biofilm_2 results demonstrate that increased internal heterogeneity over small length scales in the biomass tends to broader distributions. The distributions give unique indications for the estimation of the overall diffusion properties of diverse biofilm systems that single parameters determined by (bi.)-exp.-func. cannot express. However, the **Γ** distr. model also depicts portions of ^{1}H-NMR signals which are diffusing significantly faster than free water ($D_{water} = 2.04 \cdot 10^{-09}$ m^2/s) highlighted in gray. This portion differed for all biofilms and was especially pronounced for biofilm_1. Possible explanations for this phenomenon are convection due to temperature or enhanced diffusion by concentration gradients. Larger bulk water compartments, which were evident for biofilm_1 (Table 3), are more prone to convective transport, resulting in larger influence on D. Additionally, it is known that diffusion can increase in the presence of small concentrations of nonpolar compounds, such as methanol or acetonitrile in water mixtures (Derlacki, Easteal, Edge, Woolf, & Roksandic, 1985). The convection could also be a result of vibrations induced by the large field gradients as it is difficult to immobilize the granules and biofilm carriers.

3.5 | Correlation of diffusion and transverse relaxation

The effective $D - T_2$ relaxation correlation was measured for biofilm_1 and compared to free water (Figure 5) using a regularization parameter $\alpha = 1 \times 10^8$ and 64 steps during 2D-ILT. The peak in the upper edge of the maps is an artifact of 2D-ILT due to insufficient sampling of higher gradients. To confirm the location of the main peak in the 2D distribution, a single line of data was extracted in each dimension to produce a 1D spectrum of diffusion and relaxation as the 1D ILT is numerically more stable than the 2D (Kausik & Hurlimann, 2016). As expected, bulk water is characterized by $D_{water} = 2.4 \times 10^{-9}$ m^2/s with a reasonably narrow distribution width and by an average T_2 of 2.6 s. Compared to free water, the presence of biofilm_1 produces a significant shift of a portion of the signal to smaller D and lower T_2. Typically, T_2 and D in biofilms are less than that of bulk water (Ranzinger et al., 2016; Vogt et al., 2013). These results are consistent with previous observations. Another portion of signal attributed to the bulk water, about T_2 of 3 s, shifts toward larger D. This strongly points to convection as a possible explanation for the observation of larger diffusion coefficients in 1D diffusion experiments as well as in the correlation experiment. As mentioned earlier, this could well be due to vibrations induced by the gradients and enhanced by the biofilm as it is hard to immobilize the plastic carriers in the test tubes. It should be noted that the effect is well known and occurs in low viscosity liquids even at almost no temperature gradient if the solid structures in the sample cannot be completely immobilized.

4 | CONCLUSIONS

In this study, the water diffusion coefficients and their distributions were determined using PFG-NMR for five different biomass samples. Diffusion data were processed using conventional (bi)-exponential data analysis, the **Γ** distribution model and 2D ILT for data interpretation. Stereomicroscopic images are compared to MRI images and insights of $D - T_2$ correlation maps are introduced. The experimental results lead to the following conclusions: Similar diffusion coefficients for both data processing approaches, (bi)-exponential data analysis and **Γ** distribution model, were obtained with 5–26%

difference between D_{mean} and D_1. A better representation of the data was achieved by the **Γ** distribution function with respect to numerical reproducibility and physico-chemical interpretation. No direct correlation between D_{water} and typical biofilm properties (e.g., compactness, mineral content, VSS) was observed. D_{mean} is not sufficient to describe the mass transport in multispecies biomass. Additional information is provided by MRI images and distributions of D_{water} in the biomass obtained by **Γ** distribution model: some areas in the biofilm seem to have exhibited more restricted transport than others, associated to gas bubbles, precipitates, and changing biofilm densities. $D - T_2$ correlation maps confirmed these findings and proved a shift in T_2. More research in this field is needed, especially regarding the spatial distribution of diffusion coefficients in multispecies biomass where NMR methods are a promising approach (e.g., diffusion-weighted imaging).

ACKNOWLEDGMENTS

The authors thank all coworkers for the support in the MRI laboratory at KIT and Montana State University. The authors also thank Samuel Welker, Fabian Brunner and Oleg Tatti for the cultivation of the biofilms and maintenance of the bioreactors. MPH acknowledges the German Carl-Zeiss foundation and the Karlsruhe House of Young Scientists (KHYS) for their financial support. CMK acknowledges the support of the United States National Science Foundation Graduate Research Fellowship Program under Grant No. DGE-1049562. DFG is gratefully acknowledged for providing financial support for the joint instrumental facility Pro^{2}NMR. A special thanks to P. Galvosas (University of Wellington) and the Wellington group for the access to the Inverse Laplace transform (ILT) implementation.

ORCID

Maria P. Herrling http://orcid.org/0000-0001-6376-5439

REFERENCES

Arndt, F., Roth, U., Nirschl, H., Schütz, S., & Guthausen, G. (2016). New insights into sodium alginate fouling of ceramic hollow fiber membranes by NMR imaging. *AIChE Journal*, *62*(7), 2459–2467.

Belton, P. S. (1997). NMR and the mobility of water in polysaccharide gels. *International Journal of Biological Macromolecules*, *21*(1–2), 81–88.

Billings, N., Birjiniuk, A., Samad, T. S., Doyle, P. S., & Ribbeck, K. (2015). Material properties of biofilms-a review of methods for understanding permeability and mechanics. *Reports on Progress in Physics*, *78*(3), 036601.

Bishop, P. L., Zhang, T. C., & Fu, Y. C. (1995). Effects of biofilm structure, microbial distributions and mass transport on biodegradation processes. *Water Science and Technology*, *31*(1), 143–152.

Callaghan, P. (1991). *Principles of nuclear magnetic resonance microscopy* (p. 516). Oxford: Oxford University Press.

Callaghan, P. T. (2011). *Translational dynamics and magnetic resonance: Principles of pulsed gradient spin echo NMR*. Oxford: Oxford Press.

Callaghan, P. T., Godefroy, S., & Ryland, B. N. (2003). Diffusion-relaxation correlation in simple pore structures. *Journal of Magnetic Resonance*, *162*(2), 320–327.

Costerton, J. W., Lewandowski, Z., Caldwell, D. E., Korber, D. R., & Lappinscott, H. M. (1995). Microbial biofilms. *Annual Review of Microbiology*, *49*, 711–745.

Dammel, E. E., & Schroeder, E. D. (1991). Density of activated sludge solids. *Water Research*, *25*(7), 841–846.

de Kreuk, M. K., Pronk, M., & van Loosdrecht, M. C. M. (2005). Formation of aerobic granules and conversion processes in an aerobic granular sludge reactor at moderate and low temperatures. *Water Research*, *39*(18), 4476–4484.

Debeer, D., Stoodley, P., Roe, F., & Lewandowski, Z. (1994). Effects of biofilm structures on oxygen distribution and mass transport. *Biotechnology and Bioengineering*, *43*(11), 1131–1138.

Derlacki, Z. J., Easteal, A. J., Edge, A. V. J., Woolf, L. A., & Roksandic, Z. (1985). Diffusion coefficients of methanol and water and the mutual diffusion coefficient in methanol-water solutions at 278 and 298K. *Journal of Physical Chemistry*, *89*(24), 5318–5322.

Etterer, T., & Wilderer, P. A. (2001). Generation and properties of aerobic granular sludge. *Water Science and Technology*, *43*(3), 19–26.

Fabich, H., Vogt, S. J., Sherick, M. L., Seymour, J. D., Brown, J. R., Franklin, M. J., & Codd, S. (2012). Microbial and algal alginate gelation characterized by magnetic resonance. *Journal of Biotechnology*, *61*(3), 320–327.

Flemming, H.-C., & Wingender, J. (2010). The biofilm matrix. *Nature Reviews Microbiology*, *8*(9), 623–633.

Foerster, E., Nirschl, H., & Guthausen, G. (2017). NMR diffusion and relaxation for monitoring of degradation in motor oils. *Applied Magnetic Resonance*, *48*(1), 51–65.

Gilbert, E. M., Agrawal, S., Karst, S. M., Horn, H., Nielsen, P. H., & Lackner, S. (2014). Low temperature partial nitritation/anammox in a moving bed biofilm reactor treating low strength wastewater. *Environmental Science & Technology*, *48*(15), 8784–8792.

Guan, X. Z., Hailu, K., Guthausen, G., Wolf, F., Bernewitz, R., & Schuchmann, H. P. (2010). PFG-NMR on W1/O/W2-emulsions: Evidence for molecular exchange between water phases. *European Journal of Lipid Science and Technology*, *112*(8), 828–837.

Guimera, X., Dorado, A. D., Bonsfills, A., Gabriel, G., Gabriel, D., & Gamisans, X. (2016). Dynamic characterization of external and internal mass transport in heterotrophic biofilms from microsensors measurements. *Water Research*, *102*, 551–560.

Herrling, M. P., Guthausen, G., Wagner, M., Lackner, S., & Horn, H. (2015). Determining the flow regime in a biofilm carrier by means of magnetic resonance imaging. *Biotechnology and Bioengineering*, *112*(5), 1023–1032.

Herrling, M. P., Lackner, S., Tatti, O., Guthausen, G., Delay, M., Franzreb, M., & Horn, H. (2016). Short and long term biosorption of silica-coated iron oxide nanoparticles in heterotrophic biofilms. *Science of the Total Environment*, *544*, 722–729.

Hille, A., Neu, T. R., Hempel, D. C., & Horn, H. (2009). Effective diffusivities and mass fluxes in fungal biopellets. *Biotechnology and Bioengineering*, *103*(6), 1202–1213.

Horn, H., & Lackner, S. (2014). Modeling of biofilm systems: A review. In K. Muffler & R. Ulber (Eds.), *Productive biofilms*. Berlin: Springer-Verlag Berlin.

Horn, H., Reiff, H., & Morgenroth, E. (2003). Simulation of growth and detachment in biofilm systems under defined hydrodynamic conditions. *Biotechnology and Bioengineering*, *81*(5), 607–617.

IWA. (2006). *IWA task group on biofilm modeling: Mathematical modeling of biofilms*. London: IWA Publishing.

Juang, Y.-C., Adav, S. S., Lee, D.-J., & Tay, J.-H. (2010). Stable aerobic granules for continuous-flow reactors: Precipitating calcium and iron salts in granular interiors. *Bioresource Technology*, *101*(21), 8051–8057.

Kausik, R., & Hurlimann, M. D. (2016). Sensitivity and resolution of two-dimensional NMR diffusion-relaxation measurements. *Journal of Magnetic Resonance*, *270*, 12–23.

Kimmich, R. (1997). *NMR—Tomography, diffusometry, relaxometry*. Berlin: Springer Verlag.

Lee, J. H., Labadie, C., Springer, C. S., & Harbison, G. S. (1993). 2-Dimensional inverse laplace transform Nmr—Altered relaxation-times allow detection of exchange-correlation. *Journal of the American Chemical Society*, *115*(17), 7761–7764.

Lens, P. N. L., Gastesi, R., Vergeldt, F., van Aelst, A. C., Pisabarro, A. G., & Van As, H. (2003). Diffusional properties of methanogenic granular sludge: H-1 NMR characterization. *Applied and Environmental Microbiology*, *69*(11), 6644–6649.

Li, C. Y., Wagner, M., Lackner, S., & Horn, H. (2016). Assessing the influence of biofilm surface roughness on mass transfer by combining optical coherence tomography and two-dimensional modeling. *Biotechnology and Bioengineering*, *113*(5), 989–1000.

Loosdrecht, M. C. M. V., Nielsen, P. H., Lopez-Vazquez, C. M., & Brdjanovic, D. (2016). *Experimental methods in wastewater treatment*. Oxford: Intl Water Assn, IWA.

Manz, B., Volke, F., Goll, D., & Horn, H. (2005). Investigation of biofilm structure, flow patterns and detachment with magnetic resonance imaging. *Water Science and Technology*, *52*(7), 1–6.

McLean, J. S., Ona, O. N., & Majors, P. D. (2008). Correlated biofilm imaging, transport and metabolism measurements via combined nuclear magnetic resonance and confocal microscopy. *ISME Journal*, *2*(2), 121–131.

Metcalf, & Eddy, I. (2003). *Wastewater engineering: Treatment and reuse* (p. 2003). Boston: McGraw-Hill.

Neu, T. R., Manz, B., Volke, F., Dynes, J. J., Hitchcock, A. P., & Lawrence, J. R. (2010). Advanced imaging techniques for assessment of structure, composition and function in biofilm systems. *FEMS Microbiology Ecology*, *72*(1), 1–21.

Peulen, T.-O., & Wilkinson, K. J. (2011). Diffusion of nanoparticles in a biofilm. *Environmental Science & Technology*, *45*(8), 3367–3373.

Phoenix, V. R., & Holmes, W. M. (2008). Magnetic resonance imaging of structure, diffusivity, and copper immobilization in a phototrophic biofilm. *Applied and Environmental Microbiology*, *74*(15), 4934–4943.

Ramanan, B., Holmes, W. M., Sloan, W. T., & Phoenix, V. R. (2013). Magnetic resonance imaging of mass transport and structure inside a phototrophic biofilm. *Current Microbiology*, *66*(5), 456–461.

Ranzinger, F., Herrling, M. P., Lackner, S., Grande, V. W., Baniodeh, A., Powell, A. K., . . . Guthausen, G. (2016). Direct surface visualization of biofilms with high spin coordination clusters using magnetic resonance imaging. *Acta Biomaterialia*, *31*, 167–177.

Renslow, R. S., Majors, P. D., McLean, J. S., Fredrickson, J. K., Ahmed, B., & Beyenal, H. (2010). In situ effective diffusion coefficient profiles in live biofilms using pulsed-field gradient nuclear magnetic resonance. *Biotechnology and Bioengineering*, *106*(6), 928–937.

Röding, M., Bernin, D., Jonasson, J., Sarkka, A., Topgaard, D., Rudemo, M., & Nyden, M. (2012). The gamma distribution model for pulsed-field gradient NMR studies of molecular-weight distributions of polymers. *Journal of Magnetic Resonance*, *222*, 105–111.

Röding, M., Williamson, N., & Nydén, M. (2015). Gamma convolution models for self-diffusion coefficient distributions in PGSE NMR. *Journal of Magnetic Resonance*, *261*, 6–10.

Sanderlin, A. B., Vogt, S. J., Grunewald, E., Bergin, B. A., & Codd, S. L. (2013). Biofilm detection in natural unconsolidated porous media using a low-field magnetic resonance system. *Environmental Science & Technology*, *47*(2), 987–992.

Seymour, J. D., Gage, J. P., Codd, S. L., & Gerlach, R. (2004). Anomalous fluid transport in porous media induced by biofilm growth. *Physical Review Letters*, *93*(19), 198103.

Seymour, J. D., Gage, J. P., Codd, S. L., & Gerlach, R. (2007). Magnetic resonance microscopy of biofouling induced scale dependent transport in porous media. *Advances in Water Resources*, *30*(6–7), 1408–1420.

Stewart, P. S. (1998). A review of experimental measurements of effective diffusive permeabilities and effective diffusion coefficients in biofilms. *Biotechnology and Bioengineering*, *59*(3), 261–272.

Stewart, P. S. (2003). Diffusion in biofilms. *Journal of Bacteriology*, *185*(5), 1485–1491.

Sutherland, I. W. (2001). The biofilm matrix—An immobilized but dynamic microbial environment. *Trends in Microbiology*, *9*(5), 222–227.

Vogt, M., Flemming, H. C., & Veeman, W. S. (2000). Diffusion in *Pseudomonas aeruginosa* biofilms: A pulsed field gradient NMR study. *Journal of Biotechnology*, *77*(1), 137–146.

Vogt, S. J., Sanderlin, A. B., Seymour, J. D., & Codd, S. L. (2013). Permeability of a growing biofilm in a porous media fluid flow analyzed by magnetic resonance displacement-relaxation correlations. *Biotechnology and Bioengineering*, *110*(5), 1366–1375.

Wäsche, S., Horn, H., & Hempel, D. C. (2002). Influence of growth conditions on biofilm development and mass transfer at the bulk/biofilm interface. *Water Research*, *36*, 4775–4784.

Winkler, M. K. H., Kleerebezem, R., Strous, M., Chandran, K., & van Loosdrecht, M. C. M. (2013). Factors influencing the density of aerobic granular sludge. *Applied Microbiology and Biotechnology*, *97*(16), 7459–7468.

Wood, B. D., Quintard, M., & Whitaker, S. (2002). Calculation of effective diffusivities for biofilms and tissues. *Biotechnology and Bioengineering*, *77*(5), 495–516.